JOURNAL OF SOLID STATE CHEMISTRY **121,** 38–50 (1996)
ARTICLE NO. 0006

Magnetic Dielectric Oxides: Subsolidus Phase Relations in the $BaO:Fe_2O_3:TiO_2$ System

T. A. Vanderah, J. M. Loezos, and R. S. Roth

National Institute of Standards and Technology, Ceramics Division, Gaithersburg, Maryland 20899

Received September 29, 1995; accepted October 9, 1995

DEDICATED TO THE MEMORY OF ALEXANDER F. WELLS

The $BaO–Fe_2O_3–TiO_2$ ternary phase diagram has been investigated at 1250–1270°C in air. X-ray diffraction studies of approximately 150 polycrystalline specimens at room temperature confirmed the existence of sixteen ternary compounds. Two of these compounds, $BaFe_4Ti_2O_{11}$ and $Ba_{12}Fe_{28}Ti_{15}O_{84}$, were previously reported, four were found to be isostructural with known chemically similar compounds, and ten apparently adopt new structure-types. The crystal structures of five of the new ternary phases are briefly described. The oxidation state of iron found in this study is similar to that reported for a study of the $BaO–Fe_2O_3–SnO_2$ system in air at 1200°C. No indications of reduction of Fe^{3+} of Fe^{2+} were observed; however, oxidation to Fe^{4+} was clearly indicated in an extensive solid solution $BaTi_{1-x}Fe_xO_{3-z}$, $x = 0.06 \rightarrow 0.84$, with the hexagonal $BaTiO_3$ structure. Substantial solid solution regions were also found for the hollandite-type structure ($Ba_xFe_{2x}Ti_{8-2x}O_{16}$, $x = 1.07 \rightarrow 1.33$), and for TiO_2 dissolved in the $BaFe_{12}O_{19}$ structure (end member $BaFe_{10.8}Ti_{0.9}O_{19}$). The complexity of the $BaO–Fe_2O_3–TiO_2$ system is attributed to the coordinative versatility of Fe^{3+} in a close-packed O/Ba–O matrix and the resulting opportunity to form a wide variety of layered structures with different stacking sequences and distortions from ideal packing.

INTRODUCTION

Ceramic magnetic oxides are essential components in a wide variety of electronic applications; e.g., nearly all communications systems operating in the 50 MHz to 22 GHz region utilize coaxial circulators and isolators that contain ceramic magnets (1, 2). Materials in current use include various garnets, spinels, and the $BaFe_{12}O_{19}$-type family of hexaferrites. Improved materials would exhibit higher dielectric constants (to enhance miniaturization) without sacrificing the low dielectric losses and high saturation magnetization values ($\approx 10^3$ G) of the currently available ceramics. Hence our interest in determining phase equilibria relations in the $BaO–Fe_2O_3–TiO_2$ system, especially the crystal-chemical consequences of combining Fe_2O_3 with the technically important barium polytitanates that exhibit high dielectric constants and low dielectric losses (3, 4).

Overview of the Boundary Systems

Investigations of the binary system $BaO–TiO_2$ were first reported by Rase and Roy in 1955 (5). Since then the system has been studied in considerable detail (3, 6–10); nine compounds are now known to occur and have been structurally characterized. Three relatively ''low-temperature'' phases occur in air below 1200°C: $Ba_2Ti_5O_{12}$ is considered a metastable phase and can be formed from hydrolyzed ethoxide precursors at 650–675°C (4, 9), $BaTi_2O_5$ (4, 5, 8, 11) is stable up to ≈1100°C, and $BaTi_5O_{11}$ (4, 8, 12) was found to be stable up to ≈1200°C. Six binary compounds form in air and are stable above 1200°C including the technically important $Ba_2Ti_9O_{20}$ (2:9) (3, 4, 6, 13) and $BaTi_4O_9$ (1:4) (3, 5, 4, 14), $Ba_4Ti_{13}O_{30}$ (4:13) (3, 4, 15), $Ba_6Ti_{17}O_{40}$ (6:17) (3, 4, 16), the well-known $BaTiO_3$ in cubic/tetragonal and hexagonal forms (5, 17–19), and Ba_2TiO_4 (5, 20). The latter six compounds were expected to occur in the $BaO–Fe_2O_3–TiO_2$ system; their crystal chemistry has been reviewed by Roth *et al.* (4). Five of these six compounds adopt structural motifs made up of close-packed O/Ba–O layers with Ti occupying octahedral sites therein. The compounds differ in their layer sequencing, the patterns formed within the layers by the [TiO_6] octahedra, and the distortion of the packing from ideal. Ba_2TiO_4, the only phase that occurs between $BaTiO_3$ and BaO, is isostructural with β-K_2SO_4 and contains discrete tetrahedral [TiO_4] units that are loosely packed with Ba cations (20, 21).

The $BaO–Fe_2O_3$ system was first described by Goto and Takada (22, 23). Three equilibrium phases were reported to form in air at 1300°C: $Ba_2Fe_2O_5$, $BaFe_2O_4$, and the important permanent magnet material $BaFe_{12}O_{19}$. BaFe_2O_4 was found to dissolve to some extent in $BaFe_{12}O_{19}$ and the results also suggested a small amount of solid solution around $BaFe_2O_4$. Chemical analysis for ferrous

0022-4596/96 $12.00

ion indicated no reduction of Fe^{3+} to Fe^{2+}. $BaFe_{12}O_{19}$ is isostructural with magnetoplumbite (21, 24, 25) and is a member of the large family of ferrimagnetic hexagonal ferrites valuable in electronic devices. The numerous hexagonal ferrite structures (more than fifty), with *c*-axis dimensions up to 990 Å (21) (incommensurate?), are all built of close-packed oxygen or Ba–O layers with different stacking sequences. $BaFe_{12}O_{19}$ adopts a ten-layer structure with Fe^{3+} in octahedral (nine sites), tetrahedral (2 sites), and trigonal bipyramidal (1 site) coordination. The compound $BaFe_2O_4$ adopts a ''stuffed tridymite'' structure (26, 27) built of $[FeO_4]^{5-}$ tetrahedra with eleven- and seven-coordinated Ba^{2+}. The most recent studies of $Ba_2Fe_2O_5$ (28, 29) report a distorted perovskite-related superstructure with all iron present as Fe^{3+} in octahedral coordination. Other investigations of the $BaO–Fe_2O_3$ system in air (30–32) reported a phase $Ba_2Fe_6O_{11}$ stable below 1150°C, and that two phases, $Ba_3Fe_2O_6$ and $Ba_5Fe_2O_8$, occur between $BaFe_2O_5$ and BaO (32). However, detailed structural studies of these compounds have not appeared. Complex phase relations are observed at the 1:1 composition, $BaFeO_{3-x}$, as a function of temperature and oxygen partial pressure (33, 34); the compounds found contained varying amounts of Fe^{4+} which was quantified using wet chemical methods (33). A hexagonal phase isostructural with six-layer hexagonal $BaTiO_3$ was stable over the widest range of oxygen content ($BaFeO_{2.63–2.92}$); six other phases with perovskite-related structures were reported including a cubic form with a ~4 Å unit cell. The crystal chemistry exhibited in the binary $BaO–Fe_2O_3$ system reflects the coordinative versatility of Fe^{3+}: although octahedral coordination is often preferred by this cation, tetrahedral and five-fold coordination geometries can also be stable.

Pseudobrookite, Fe_2TiO_5, is the only phase reported to form in the $TiO_2–Fe_2O_3$ binary system (23, 35, 36). The crystal structure of pseudobrookite features Ti^{4+} in octahedral coordination while that of Fe^{3+} is (4 + 2) and can be considered as a highly distorted octahedron or a distorted tetrahedron plus two (21). At 1200°C in air very little solid solution around pseudobrookite was indicated, limited solubility of hematite in TiO_2 was observed (~2 mol% Fe_2O_3), and approximately 13 mol% TiO_2 was found to dissolve in Fe_2O_3 (35). According to electron microscopy studies (37), rutile samples containing 8–16 wt% hematite contained a series of rutile crystallographic shear structures (''swinging-shear'' structures). Both TiO_2 and corundum-type Fe_2O_3 can be considered distorted hexagonally close-packed structures with 1/2 and 2/3 of the octahedral sites occupied by metals, respectively; Baur has described the unique properties of the sphere-packing arrangement in TiO_2 (38). In rutile, strings of opposite-edge-sharing $[TiO_6]$ octahedra are connected via vertex sharing to form a three-dimensional network while in corundum the octahedra share faces, edges, and vertices.

Previously Reported Ternary Compounds

According to the current literature three compounds have been reported in the $BaO–Fe_2O_3–TiO_2$ system. In 1974 Haberey and Velicescu (39) reported the synthesis (1300°C, air) of $BaFe_4Ti_2O_{11}$ (''1:2:2'') as the first example of a neutral, isolated ''R-block'' structure: R-blocks (general formula $(BaFe_6O_{11})^{2-}$) combine with spinel-like ''S-blocks'' (general formula $(Fe_6O_8)^{2+}$) in various permutations to form the structures of the numerous hexagonal ferrites, including magnetoplumbite-type $BaFe_{12}O_{19}$. The R-block structural unit contains close-packed Ba–O and oxygen layers in an *hcp* array that results in pairs of face-sharing $[FeO_6]$ octahedra as well as fivefold coordinated sites for iron. $BaFe_4Ti_2O_{11}$ (1:2:2) was reported to crystallize in space group $P6_3/mmc$ according to X-ray diffraction studies of polycrystalline samples using the Guinier method (39). A subsequent powder neutron diffraction and ^{57}Fe Mössbauer study by Obradors *et al.* (40) confirmed this result and concluded that the five-coordinated metal site was occupied only by Fe^{3+} with some preferential ordering of Fe^{3+} and Ti^{4+} among the remaining two octahedral sites. The fivefold site was found to result from static disorder between two distorted tetrahedral sites to form a trigonal bypyramid, as is also found in the parent $BaFe_{12}O_{19}$; the authors concluded that all iron was present in the 3+ oxidation state. The crystal structure of $BaFe_4Ti_2O_{11}$ is illustrated in Fig. 1 (41). The tin congener of this compound, $BaFe_4Sn_2O_{11}$, has also been prepared (42). Another ternary compound $BaFe_2TiO_6$ (''1:1:1''), prepared at 1350°C under ~2 atm oxygen, was reported by Belikaya *et al.* in 1985 (43). The reported X-ray powder diffraction pattern was indexed on a tetragonal unit cell ((44) PDF 39-810); however, to our knowledge no detailed structural study or other reports of this phase have subsequently appeared in the literature. The preparation and single-crystal X-ray structure determination of a third compound in the $BaO–Fe_2O_3–TiO_2$ system, $Ba_{12}Fe_{28}Ti_{15}O_{84}$ (''12:14:15''), was reported in 1991 by Grey *et al.* (45). Crystals were grown by slow-cooling (from 1300°C) a 1:2:2 mixture of $BaCO_3$, Fe_2O_3, and TiO_2 with KBO_2 as a flux. The 12:14:15 compound crystallizes in space group $C2/m$ with an 8-layer *cchccccch* stacking sequence of O/Ba–O close-packed layers. The structure can be described as an intergrowth of perovskite-like and spinel-like blocks with a high degree of ordering of Ti^{4+} into the former and Fe^{3+} into the latter structural units. The observed bond distances, the stoichiometry indicated in the structural refinement, and the results of microprobe analysis were all consistent with the title formula and the presence of iron in the 3+ oxidation state. The authors mention that the crystals assumed a preferential orientation when placed near a hand magnet.

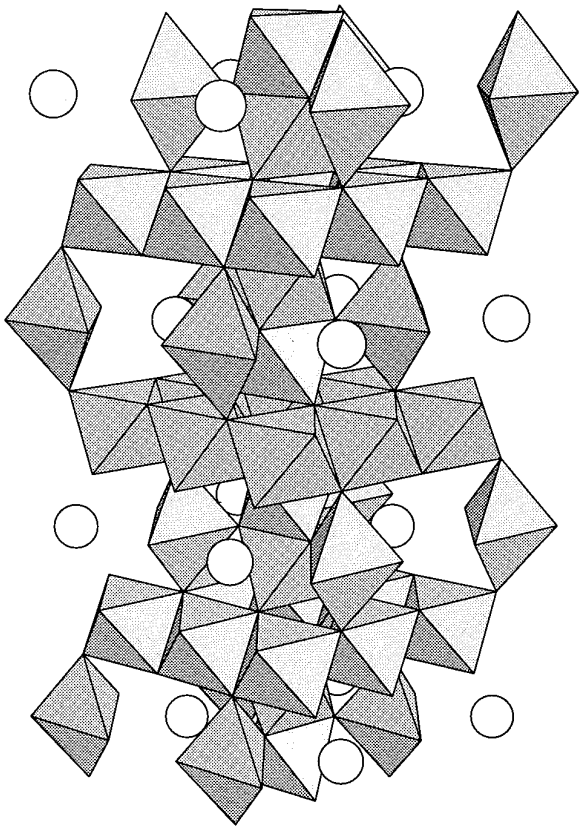

FIG. 1. The hexagonal crystal structure of $BaFe_4Ti_2O_{11}$ (1:2:2) (Table 1) (after 40), perspective view approximately along the ⟨110⟩ direction. The large spheres are Ba cations; Fe^{3+} occupies the five-coordinated trigonal bipyramidal sites while the octahedral sites contain mixed Fe^{3+}/Ti^{4+}. Along the *c* direction close-packed layers containing octahedral metal sites are seen to alternate with slabs containing trigonal bipyramids and pairs of face-sharing octahedra. The synthesis of this compound (39) was the first example of a neutral, isolated R-block, $(BaFe_6O_{11}))^{2-}$, one of two basic building blocks of the large family of technically important hexaferrites (21, 40). The R-block-type structure of $BaFe_4Ti_2O_{11}$ shown here is a portion of the magnetoplumbite-type structure of the hexaferrite $BaFe_{12}O_{19}$.

Predicted Ternary Compounds

By analogy with other chemically similar ternary systems, a number of compositions in the $BaO–Fe_2O_3–TiO_2$ system were initially chosen as potential locations of isostructural compounds. As in the $BaO–Fe_2O_3–SnO_2$ system (42) and also the $BaO–Al_2O_3–TiO_2$ system (4), compound formation at 3:5:1 ($Ba_3Fe_{10}TiO_{20}$) and near hollandite ($Ba_xFe_{2x}Ti_{8-2x}O_{16}$) was plausible; a compound at 3:5:1 is also known in the $SrO–Al_2O_3–TiO_2$ system (46), and the hollandite structure also forms in the $Ba–Cr^{3+}–Sn^{4+}–O$ (47) system. In addition, in the aluminum system compounds form at 4:1:10, 2:3:4, and 1:3:1 $BaO:Al_2O_3:TiO_2$ (4). The 4:1:10 compound, $Ba_4Al_2Ti_{10}O_{27}$, is isostructural with a compound in the $BaO–ZnO–TiO_2$ system, $Ba_4ZnTi_{11}O_{27}$ (4, 48), also containing a 4:12 ratio of large to small cations. Another compound isostructural with $K_2Ti_6O_{13}$ was found in the Zn system, $Ba_2ZnTi_5O_{13}$ (4, 48), and also in the $BaO–MgO–TiO_2$ system, $Ba_2MgTi_5O_{13}$ (4). By inference a compound in the iron system at 2:1:4 ($Ba_2Fe_2Ti_4O_{13}$) with the same ratio of large cations, small cations, and anions was deemed possible; interestingly, a compound at 2:1:4 in the $BaO–Al_2O_3–TiO_2$ system does *not* form (4). Lastly, if substantial reduction of iron to the divalent state was encountered, a compound at 1:3:6 ($BaFe^{2+}_6Ti_6O_{19}$) by analogy with $BaFe_{12}O_{19}$ and $BaMg_6Ti_6O_{19}$ (4) could form. In summary, a total of seven possible isostructural compounds in addition to the three previously reported phases served as synthetic starting points for the present investigation of phase relations in the $BaO–Fe_3O_3–TiO_2$ system.

EXPERIMENTAL METHODS

Approximately 150 polycrystalline specimens were prepared by solid-state reaction of reagent-grade $BaCO_3$, Fe_2O_3, and phosphate-free TiO_2 in air. Before each heating the ≈3-g samples were mixed by grinding with an agate mortar and pestle for 15–20 min, pressed into pellets, and placed on sacrificial powder of the same stoichiometry in an alumina combustion boat. Samples were first calcined at 1000°C for 48 h followed by multiple 1-week heatings at 1250–1270°C; products were step-cooled to 750°C followed by air quenching. The attainment of equilibrium conditions was assumed when the X-ray powder diffraction patterns obtained under ambient conditions exhibited no further changes; three to five heatings were typically required. The colors of the specimens in this system ranged from light brown near the $BaO–TiO_2$ binary to brown–black near the $BaO–Fe_2O_3$ binary. Approximately 100 crystal-growth experiments, all yielding deep red products, were carried out by melting/partially melting neat samples and also by using $K_2O–B_2O_3$ fluxes. Melting experiments were carried out in Pt capsules (diameter 2.5 mm, partly open to the air) by soaking at temperatures ranging from 1275 to 1390°C followed by various cooling regimes including quenching. Crystal growth experiments using $K_2O–B_2O_3$ fluxes ($0.38K_2O:0.62B_2O_3$, m.p. 787°C and $1K_2O:1B_2O_3$, m.p. 815°C) were carried out in welded Pt capsules and in lidded Pt crucibles. The best results were obtained by slow-cooling (1°C/h) partial melts to below the solidus temperatures. Although the $BaO–Fe_2O_3–TiO_2$ samples were observed to be highly soluble in the $K_2O–B_2O_3$ fluxes (e.g., complete dissolution at 1000°C of a 20 wt% charge:flux mixture), the very high vaporization rate of the fluxes, even with lidded and welded containers, necessitated low soak temperatures (1000°C) and fast cooling rates (10°C/h) which often yielded poor-quality crystals.

Polycrystalline samples were characterized by X-ray

powder diffraction using an automated vertical diffractometer equipped with a theta compensating slit and a graphite postmonochromator. Data were collected using Cu$K\alpha$ radiation in steps of 0.02° 2Θ at 2 s/step and were corrected for systematic error using Si and W as external calibrants. Single crystals were characterized by the precession method using Zr-filtered Mo$K\alpha$ radiation. Whenever possible, unit cells determined from precession photographs were used as initial parameters in least-squares refinements (49) using the observed powder patterns of previously unreported phases.

Qualitative analysis for tetravalent iron was performed by adding a ≈30-mg Ba–Fe–Ti–O sample to colorless concentrated hydrobromic acid to detect the generation of red liquid bromine ($Fe^{4+}_{(aq)} + Br^{-}_{(aq)} \rightarrow Fe^{3+}_{(aq)} + \frac{1}{2}Br_{2(l)}$) by visual inspection.

RESULTS AND DISCUSSION

The $BaO–Fe_2O_3–TiO_2$ phase diagram was found to be remarkably complex and results to date are given in Figs. 2 and 3. Extensive solid solution regions were found to exist for hexagonal $BaTiO_3$, the hollandite-type structure, and the technically important ferrite $BaFe_{12}O_{19}$. Under the synthetic conditions of this study the formation of sixteen ternary compounds (Table 1)—fourteen in addition to two of the previously reported phases—was confirmed. Except for the hollandite system, solid solution of the various ternary compounds was not investigated per se in the present study and hence the compounds are represented as points in Figs. 2 and 3. Likewise, solid solution in the boundary binary systems is not indicated except where specifically investigated. The solidus minima in the system were observed near 1275°C in the vicinity of the 3:2:3 and 6:2:7 compounds and near the 1:1:1 composition. In this study the 1:1:1 composition was found to occur in a three-phase field even after 7 weeks of heating; no compound corresponding to $BaFe_2TiO_6$ (43) was observed. The X-ray powder diffraction pattern reported for $BaFe_2TiO_6$ ((44) PDF 39-810) contains strong lines that overlap with those observed for $Ba_{12}Fe_{28}Ti_{15}O_{84}$ (12:14:15); however, the entire reported pattern could not be accounted for assuming a mixture of the phases observed in the present study. In air the 1:1:1 composition was observed here to melt at ≈1280°C whereas the preparation temperature for $BaFe_2TiO_6$ under oxygen was reported to be 1350°C (43).

Ternary Phases Found in the $BaO–Fe_2O_3–TiO_2$ System

Isostructural compounds. In addition to two ($BaFe_4Ti_2O_{11}$ and $Ba_{12}Fe_{28}Ti_{15}O_{84}$) of the three previously reported phases, four of the seven predicted isostructural compounds were found to exist under the conditions of this study at the compositions 1:1:5.5→1:1:4, 2:1:4, 3:5:1, and 4:1:10 $BaO–Fe_2O_3–TiO_2$ and are described below.

A hollandite-type solid solution was observed in the approximate compositional range 1:1:5.5→1:1:4 ($Ba_xFe_{2x}Ti_{8-2x}O_{16}$, $x = 1.07 \rightarrow 1.33$) (51). In the hollandite structure (52) the smaller cations occupy octahedra that share edges and vertices to form a three-dimensional framework with channels to accommodate the larger Ba ions; analysis of the structure is problematic in that the (probably incommensurate) ordering of the large channel ions is out of registry with the framework and/or other channels. The observed X-ray powder diffraction patterns therefore exhibit broad, weaker peaks in addition to a sharper pattern that can be indexed on the basis of the unit cells given in Table 1. The space group $I2/m$ has been used to facilitate comparison with the tetragonal parent structure ($I4/m$; $a \approx 10$, $c \approx 3$ Å for $A_2B_8[O(OH)]_{16}$) (52). As can be seen in Table 1, as the x value increases with greater filling of the channel sites, the monoclinic distortion observed in the room-temperature X-ray powder diffraction pattern becomes markedly larger.

$Ba_2Fe_2Ti_4O_{13}$ (2:1:4) crystals were obtained from a partial melt of 1:2:2 ($BaFe_4Ti_2O_{11}$) at 1390°C; a detailed structural study by single-crystal X-ray and powder neutron diffraction and characterization of magnetic and dielectric properties are reported elsewhere (53, 54). The 2:1:4 compound was confirmed to be isotypic with $K_2Ti_6O_{13}$, $Ba_2ZnTi_5O_{13}$, and $Ba_2MgTi_5O_{13}$ with a structure intermediate between close-packed and open-framework. Fe^{3+} and Ti^{4+} are partially ordered among highly distorted octahedra. As shown in Fig. 4, repeating units of three opposite-edge-sharing octahedra are vertex-linked in a pattern that creates open channels to accommodate the Ba ions in (8 + 3)-coordinated tricapped pseudo-cubic sites. Magnetic measurements indicated complex, field-dependent behavior characteristic of weak exchange interactions, however no magnetic ordering was observed in the neutron diffraction studies down to 13 K. Preliminary assessment of dielectric properties indicated a relative permittivity of ≈28 and that dispersion was low enough for TE_0 resonance to be observed at 10.34 GHz.

Crystals of the compound found at 3:5:1, $Ba_3Fe_{10}TiO_{20}$ (54), were obtained by prolonged heating with minimal melting of the stoichiometric compound at 1285°C. Refinement of the structure by single-crystal X-ray diffraction (55) confirmed that $Ba_3Fe_{10}TiO_{20}$ is isostructural with the corresponding compounds in the Ba–Fe–Sn^{4+}–O and Ba–Al–Ti–O systems and also with $Pb_3Al_{10}GeO_{20}$ and $Pb_3Al_{10}SiO_{20}$ (56). The structure contains four crystallographic sites for the smaller cations, two with tetrahedral coordination occupied by Fe^{3+} and two octahedral sites with mixed Fe^{3+}/Ti^{4+} occupation. As shown in Fig. 5, the structural pattern features portions of close-packed layers (units of four edge-sharing octahedra) interconnected by vertex-

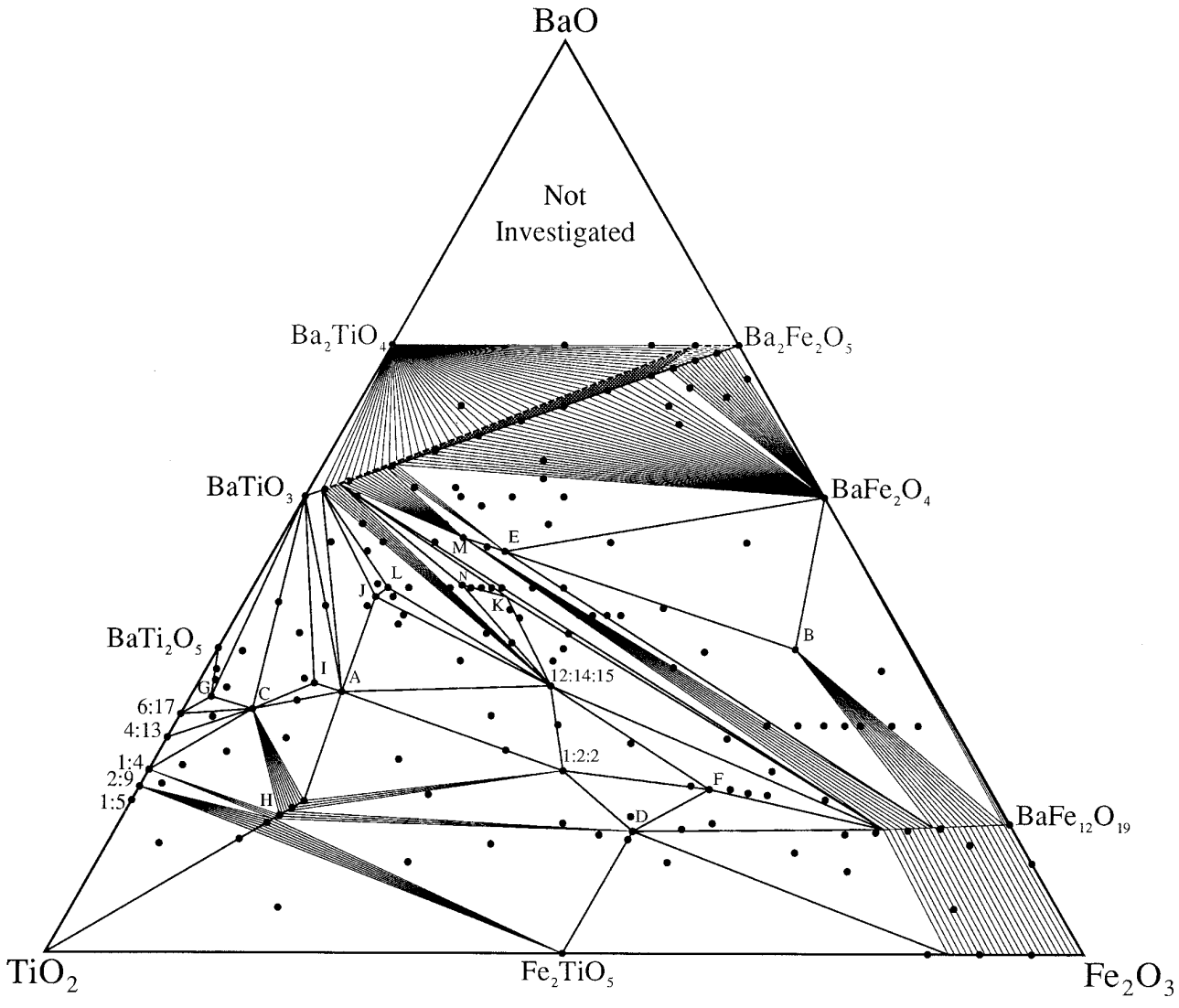

FIG. 2. $BaO–Fe_2O_3–TiO_2$ phase diagram (air, 1250–1270°C) (50). The compositions of the ternary phases found in the system are listed in Table 1.

sharing [FeO_4] tetrahedra to form a framework-like structure with channels accommodating the Ba ions.

The compound $Ba_4Fe_2Ti_{10}O_{27}$ (54), found at the 4 : 1 : 10 composition, was grown in single-crystal form by slow-cooling an off-stoichiometric partial melt from 1340°C. Refinement of the structure by single-crystal X-ray diffraction (55) confirmed that this phase is isotypic with the Al^{3+} analog first reported by Schmachtel and Müller-Buschbaum (57) and with $Ba_4ZnTi_{11}O_{27}$. The structure is shown in Fig. 6 and is built of close-packed O/Ba–O layers in a distorted *hcp* 8L sequence reminiscent of the structural theme of the barium polytitanates (4). Fe^{3+} and Ti^{4+} are distributed among ten octahedral sites with some preferential ordering. In this structure Fe^{3+} exhibits six-coordination only.

Compounds with new structure-types. In the subsolidus investigation of the $BaO–Fe_2O_3–TiO_2$ system the existence of ten ternary phases with apparently new structure types was clearly indicated. These compounds are listed in Table 1 and included in Figs. 2 and 3; their chemical compositions have been estimated by the disappearing phase method (58) and in nearly all cases the preparation of single-phase (by X-ray powder diffraction) specimens was eventually attained. X-ray powder diffraction analysis in this system required detailed attention and frequent instrument calibration-checks as the phases exhibit highly complex patterns that are "similar but different." Most of the new compounds appear to share a similar structural theme reminiscent of the known interior compounds at 12 : 14 : 15 and 1 : 2 : 2 $BaO–Fe_2O_3–TiO_2$; i.e., close-packed layer struc-

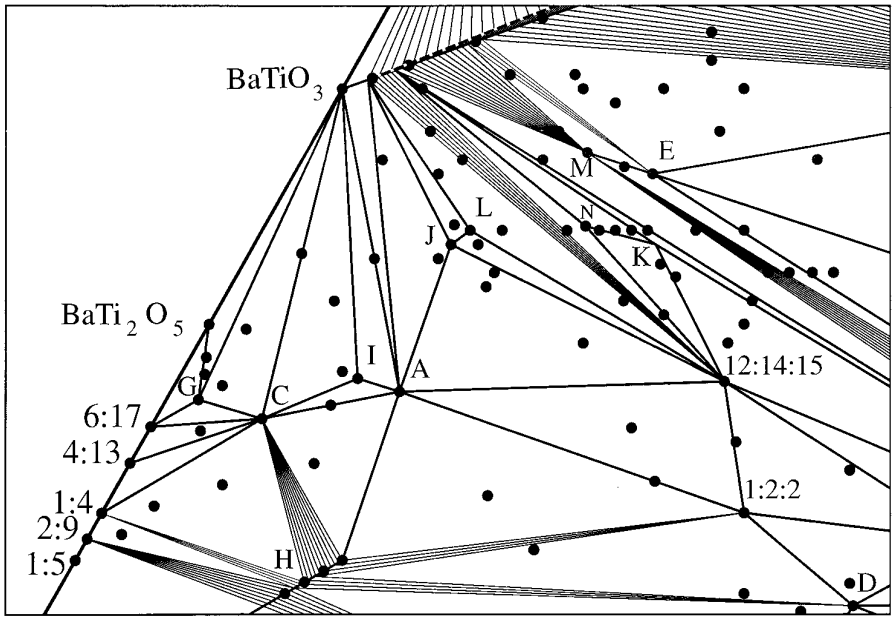

FIG. 3. Expanded region of the $BaO–Fe_2O_3–TiO_2$ phase diagram from Fig. 1 showing locations of eleven of the new ternary phases (see Table 1).

tures combining elements of the $BaFe_{12}O_{19}$ and the cubic or hexagonal $BaTiO_3$ structures. Many of the powder diffraction patterns exhibited coincidential or nearly coincidental strongest lines with more subtle but distinct differences in the weaker diffraction peaks; an ideal hexagonal parent-cell with $a \sim 5.75$ and $c \sim 2.35n$ Å, where n is the number of close-packed O/Ba–O layers, was repeatedly suggested by patterns observed in precession photographs and powder diffraction data. Crystals deemed suitable for structure determination by single-crystal methods have been obtained for seven of the ten phases. Detailed structural studies are in progress and will be reported elsewhere along with the results of neutron diffraction studies to distinguish Fe/Ti site occupations and characterization of dielectric and magnetic properties.

A preliminary determination of the structure of $\approx Ba_3Fe_{24}Ti_7O_{53}$ (“3:12:7”) has been completed by single-crystal X-ray diffraction methods using crystals grown by slow-cooling a near-stoichiometric melt from 1450°C. The structure is a close-packed 8L arrangement with eighteen Fe^{3+}/Ti^{4+} sites, two of which feature tetrahedral coordination and appear to be preferentially occupied by Fe^{3+}. The structure is shown in Fig. 7. Crystals of this compound were attracted to a hand magnet and characterization of its physical properties is in progress; a more complete report will appear elsewhere. Similar magnetic properties were observed for the “1:6:3” ($\approx Ba_2Fe_{12}Ti_3O_{26}$) crystals and, to some degree approximately correlating with Fe content, for all of the crystals obtained of the new phases listed in Table 1.

Hexagonal $BaTiO_3$-Type Solid Solution

Iron substitution into the $BaTiO_3$ system was observed to stabilize the hexagonal $BaTiO_3$ structure (18, 19) as opposed to the cubic/tetragonal perovskite-like arrangement (26, 59). As seen in Fig. 8, the connectivity in hexagonal $BaTiO_3$ is substantially different from that in the perovskite derivatives: six close-packed layers per unit cell versus three, *cch* stacking sequence of close-packed layers versus *ccc*, and the occurrence of face-sharing pairs of octahedra versus vertex-only sharing octahedra in perovskite (26). An extensive solid solution with the hexagonal $BaTiO_3$ structure, $BaTi_{1-x}Fe_xO_{3-z}$, $x = 0.06 \rightarrow 0.84$, was observed in the present study. Qualitative tests for Fe^{4+} were positive for these specimens, suggesting behavior analogous to that observed for the $Ba_2Fe_2O_5–BaSnO_3$ system (42), in which an extensive perovskite-type solid solution was observed and was attributed to the oxidation of Fe^{3+} to Fe^{4+}. Cadée and Ijdo also report a large triangular two-phase region bounded by $BaFe_2O_4$, $BaSnO_3$, and $Ba_2Fe_2O_5$ similar to the present results in the $BaO–Fe_2O_3–TiO_2$ system (Fig. 2).

A substantial variation in lattice parameters with composition was observed for the hexagonal $BaTiO_3$-type solid solution. The unit cell dimensions and cell volume are plotted as a function of the x value in Fig. 9. Substitution of iron into $BaTiO_3$ implies the oxidation of Fe^{3+} to Fe^{4+} and/or the formation of anion vacancies (□) according to

$$BaTi^{4+}_{1-x-y}Fe^{3+}_xFe^{4+}_yO_{3-1/2x}\square_{1/2x}.$$

TABLE 1
Ternary Phases Found in the $BaO–Fe_2O_3–TiO_2$ System in Air, 1250–1270°C

	Compound	Composition	Space group	Unit cell	# Layers[a]	References/status
	1:2:2	$BaFe_4Ti_2O_{11}$	$P6_3/mmc$	a = 5.843(1), c = 13.608(2) Å	6,*c*	(39, 40) New structure-type
	12:14:15	$Ba_{12}Fe_{28}Ti_{15}O_{84}$	$C2/m$	a = 9.988(7), b = 17.298(9), c = 19.17(2) Å, β = 99.33(6)°	8,*c*	(45) New structure-type
H	1:1:5 hollandite	$Ba_xFe_{2x}Ti_{8-2x}O_{16}$ x = 1.143	$I2/m$	a = 10.129(4), b = 2.967(1), c = 10.031(4) Å, β = 90.40(2)°	—	This work, (51) Isostructure
H	1:1:4 hollandite	$Ba_xFe_{2x}Ti_{8-2x}O_{16}$ x = 1.333	$I2/m$	a = 10.235(5), b = 2.979(1), c = 9.909(5) Å, β = 90.99(2)°	—	This work, (51) Isostructure
A	2:1:4	$Ba_2Fe_2Ti_4O_{13}$	$C2/m$	a = 15.216(1), b = 3.8979(3), c = 9.1350(6) Å, β = 98.460(7)°	—	(53, 54) Isostructure
B	3:5:1	$Ba_3Fe_{10}TiO_{20}$	$I2/m$	a = 15.379(1), b = 11.837(1), c = 5.1845(4) Å, β = 91.237(6)°	—	(54, 55) Isostructure
C	4:1:10	$Ba_4Fe_2Ti_{10}O_{27}$	$C2/m$	a = 19.830(2), b = 11.449(1), c = 9.909(1) Å, β = 109.19(1)°	8,*a*	(54, 55) Isostructure
D	"3:12:7"	$\approx Ba_3Fe_{24}Ti_7O_{53}$	$C2/m$	a = 19.400(2), b = 20.269(1), c = 10.084(1) Å, β = 105.30(1)°	8,*a*	This work; single-crystal structural study in progress
E	"4:2:3"	$\approx Ba_4Fe_4Ti_3O_{16}$	Hexagonal[b]	a = 5.7618(3), c = 23.738(1) Å	10,*c*	This work; single-crystal structural study in progress
F	"1:6:3"	$\approx Ba_2Fe_{12}Ti_3O_{26}$	$C2/m$[b]	a = 10.024(1), b = 17.378(1), c = 35.373(3) Å, β = 90.762(8)°	15,*c*	This work; single-crystal structural study in progress
G	"14:1:35"	$\approx Ba_{14}Fe_2Ti_{35}O_{87}$	*Pncm* or *Pnc2*[b]	a = 9.8556(8), b = 11.3887(7), c = 23.322(2) Å	10,*c*	This work; single-crystal structural study in progress
I	"8:3:16"	$\approx Ba_8Fe_6Ti_{16}O_{49}$	$P6_3/mcm$[b]	a = 9.9917(4), c = 42.252(2) Å	18,*c*	This work; single-crystal structural study in progress
J	"3:1:4"	$\approx Ba_3Fe_2Ti_4O_{14}$	$C2/m$[b]	a = 9.947(1), b = 5.7456(7), c = 42.364(6) Å, β = 94.70(1)°	18,*c*	This work; single-crystal structural study in progress
K	"8:5:8"	$\approx Ba_8Fe_{10}Ti_8O_{39}$	Pseudotrigonal[b]	a = 9.977, c = 61.41 Å	26,*c*	This work; single-crystal structural study in progress
L	"6:2:7"	$\approx Ba_6Fe_4Ti_7O_{26}$	Pseudotrigonal[b]	a = 5.736, c = 98.84 Å	42,*c*	This work; crystal growth in progress for better crystals
M	"8:3:6"	$\approx Ba_8Fe_6Ti_6O_{29}$	Trigonal[c]	a = 5.7538(3), c = 61.482(4) Å	26,*c*	This work; crystal growth in progress.
N	"2:1:2"	$\approx Ba_2Fe_2Ti_2O_9$	?	?	?	This work; crystal growth in progress

[a] The close-packing direction is indicated after the number of layers.

[b] The unit cell given was suggested by analysis of polaroid precession photographs and can be used to index the X-ray powder diffraction pattern but may not be the correct cell. Single-crystal structural studies are in progress.

[c] Crystals of this phase have not yet been obtained; however, its powder pattern can be indexed on the unit cell given. Note the similarity of this cell to that of "8:5:8" (a axes related by $\sqrt{3}$). Comparison of the powder diffraction patterns of the two phases suggests that they possess distinctly different but related structures.

The behavior of the lattice parameters of the solid solution as seen in Fig. 9 suggests that more than one process contributes to the formation of the solid solution, that these processes affect the lattice differently, and that the dominant process changes near an x value of 0.4. In studies of hexagonal $BaFeO_{3-x}$ prepared under oxygen, Mori reports (33) a marked contraction in both the a and c axes with increasing Fe^{4+} concentration as quantified by chemical analysis. As seen in Fig. 9, a steady contraction of the hexagonal $BaTi_{1-x}Fe_xO_{3-z}$ unit cell parameters is observed above x values of 0.4 and is likely attributable to increasing oxidation to the smaller tetravalent iron. The values for the x = 0.67 composition are seen to fall below the curves; this particular specimen was heated five times (as compared to three for the other samples) and likely contains more Fe^{4+}. Samples with the highest x values were observed to react the most vigorously to produce bromine and the X-ray diffraction pattern of the end member, x = 0.84, degraded over time upon exposure of the specimen to air. As seen in Fig. 9, the behavior below x values near 0.4 is markedly different: upon initial substitution of iron in the hexagonal $BaTiO_3$ structure, the a axis contracts whereas the c axis expands, resulting in a slight overall increase in cell volume up to ~20 mol% Fe. These effects may be attributable to the formation of anion vacancies about which the structure expands anisotropically; how-

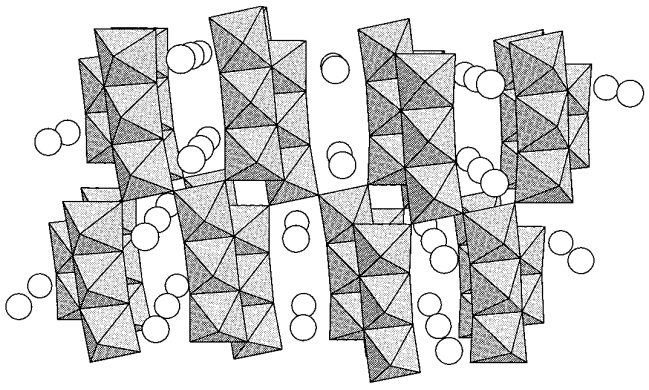

FIG. 4. The monoclinic crystal structure of $Ba_2Fe_2Ti_4O_{13}$ (2:1:4) (Compound A, Table 1) (after 53), perspective view approximately along the *b* direction. Large spheres are Ba cations. Fe^{3+} and Ti^{4+} are partially ordered among highly distorted octahedra. As seen here along the *b* direction, repeating units of three opposite-edge-sharing octahedra share edges with each other to form infinite corrugated ribbons three-octahedra wide. The ribbons are interconnected by vertices creating open channels to accommodate Ba ions in (8 + 3)-coordinated tricapped pseudo-cubic sites. $Ba_2Fe_2Ti_4O_{13}$ is isotypic with $K_2Ti_6O_{13}$, $Ba_2ZnTi_5O_{13}$, and $Ba_2MgTi_5O_{13}$.

ever, detailed structural studies would be required to confirm this interpretation. Above $x \approx 0.4$, oxidation to tetravalent iron appears to become the dominant chemical mechanism for formation of the solid solution.

The existence of a single-phase region for the hexagonal $BaTiO_3$ structure, shown in Fig. 2 as extending up to the Ba_2TiO_4–$Ba_2Fe_2O_5$ composition line, was inferred from the indicated two-phase nature of the three specimens along this line. The position of the single-phase region suggests that the hexagonal $BaTiO_3$ structure will tolerate vacancies at the octahedral cation sites.

Above $x = 0.84$ in the $BaTi_{1-x}Fe_xO_{3-z}$ solid solution the hexagonal $BaTiO_3$-type structure was not stable and converted to a lower-symmetry form observed in the range $x = 0.88 \rightarrow 0.98$. The X-ray powder diffraction pattern for this structure was very different from that observed for the end member $Ba_2Fe_2O_5$, which was in agreement with that reported by Parras *et al.* ((29, 44) PDF 39-1296). The powder pattern for the lower symmetry $BaTi_{1-x}Fe_xO_{3-z}$ solid solution was similar to that reported for Ba $Fe^{3+}_{0.66}Fe^{4+}_{0.34}O_{2.67}$ ((33, 44) PDF 20-129), referred to as the "Triclinic II" phase by Mori (33) and prepared in polycrystalline form by heating $BaFe_2O_5$ in oxygen at 400–500°C. However, the entire diffraction pattern observed in our study for the low-symmetry solid solution could not be accounted for using the unit cell reported for the Triclinic II phase (33). Detailed structural studies using single-crystal and/or powder neutron diffraction methods are needed to characterize the $BaTi_{1-x}Fe_xO_{3-z}$ solid solution for $x = 0.88 \rightarrow 0.98$.

$BaFe_{12}O_{19}$-Type Solid Solution

In the present study a substantial solid solution of TiO_2 in the $BaFe_{12}O_{19}$ structure was observed. In Fig. 2, the solution has been drawn along the line $BaFe^{3+}_{12-(4/3)x}Ti^{4+}_xO_{19}$ with an end member $\approx BaFe_{10.8}Ti_{0.9}O_{19}$. Along this line, iron vacancies form to permit the aliovalent substitution of titanium. The other possible mechanisms, namely, barium vacancy formation ($Ba_{1-1/2x}Fe_{12-x}Ti_xO_{19}$) or excess oxygen ($BaFe_{12-x}Ti_xO_{19+1/2x}$), were considered less likely crystal-chemically and were inconsistent with the phase assemblages observed in compositions near the solid solution line. Heimke, in a study of the effects of substituents on the magnetic properties of $BaFe_{12}O_{19}$ (60), reported that the composition $BaTiO_3 \cdot 5Fe_2O_3$ was single-phase magnetoplumbite. This result is in fair agreement with the present results. Cadée and Ijdo (42) also reported substantial substitution of SnO_2 into the $BaFe_{12}O_{19}$ structure with marked changes in the unit cell and intensities of the diffraction

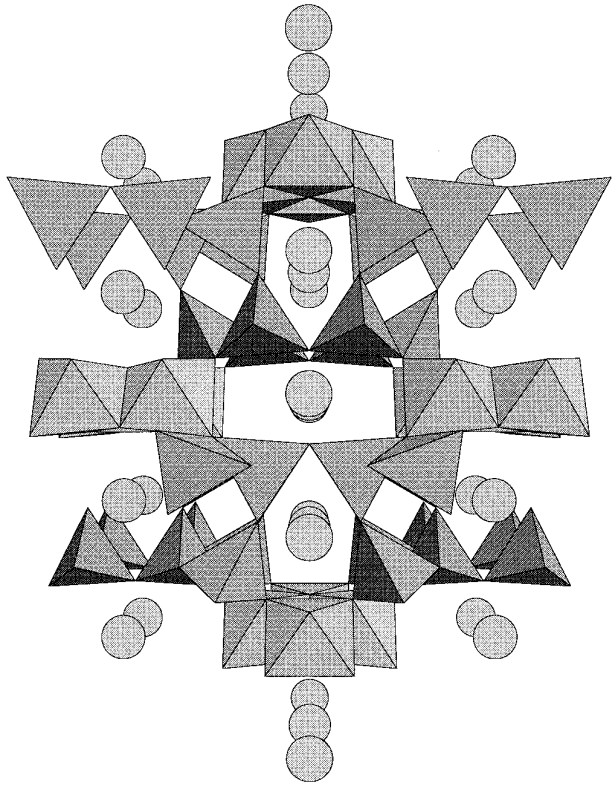

FIG. 5. The monoclinic crystal structure of $Ba_3Fe_{10}TiO_{20}$ (3:5:1) (Compound B, Table 1) (after 55), perspective view approximately along the *c* direction. Large spheres are Ba cations. This structure contains tetrahedral Fe^{3+} and two octahedral sites with mixed Fe^{3+}/Ti^{4+} occupation. The structural pattern features portions of close-packed layers (units of four edge-sharing octahedra) interconnected by vertex-sharing tetrahedra to form a framework-like structure with channels accommodating the Ba ions. This compound is isostructural with $Ba_3Fe_{10}SnO_{20}$, $Ba_3Al_{10}TiO_{20}$, $Pb_3Al_{10}GeO_{20}$, and $Pb_3Al_{10}SiO_{20}$.

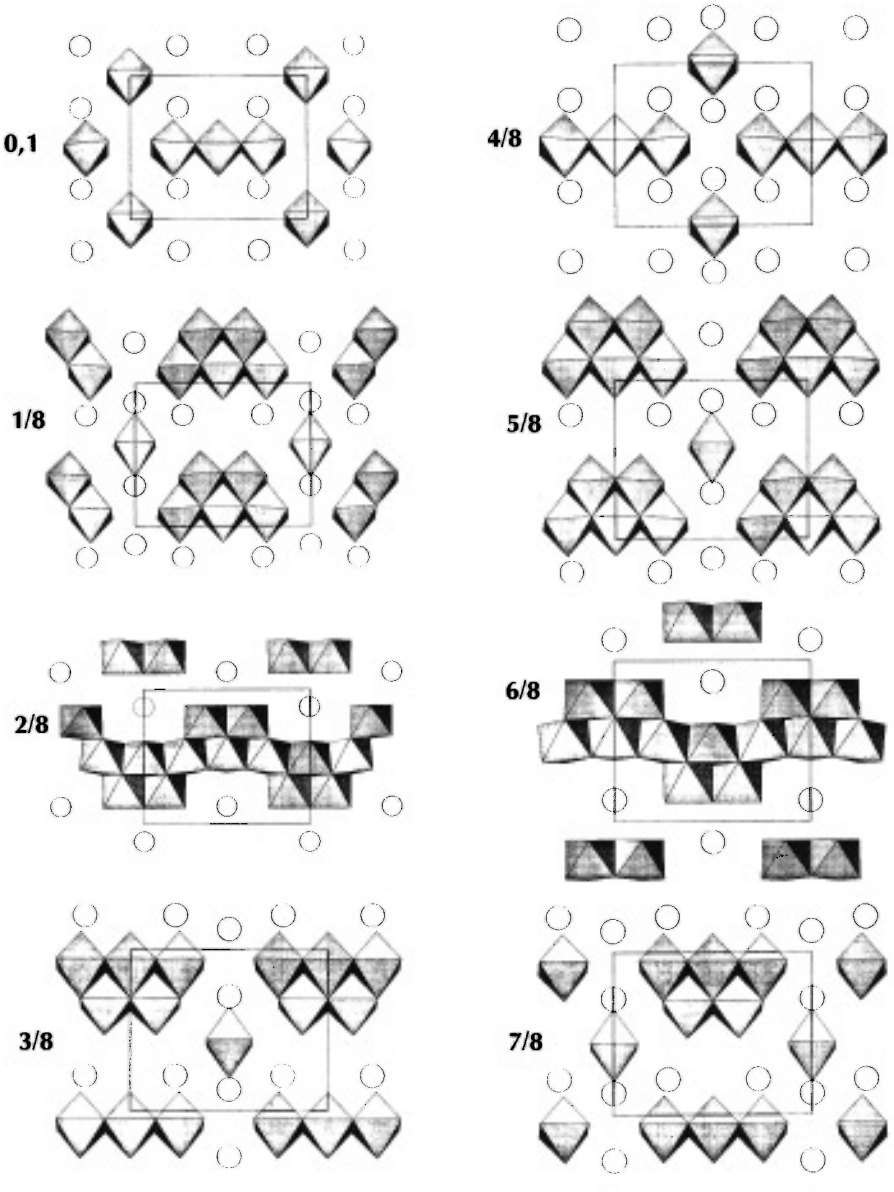

FIG. 6. The monoclinic crystal structure of $Ba_4Fe_2Ti_{10}O_{27}$ (4:1:10) (Compound C, Table 1) (after 55) viewed as layers along the distorted-close-packing *a* direction. Large spheres are Ba cations. The structure is built of close-packed O/Ba–O layers in a distorted *hcp* 8L sequence reminiscent of the structural theme of the barium polytitanates (4). Fe^{3+} and Ti^{4+} are distributed among ten octahedral sites with some preferential ordering. In this structure Fe^{3+} exhibits six-coordination only. $Ba_4Fe_2Ti_{10}O_{27}$ is isostructural with $Ba_4Al_2Ti_{10}O_{27}$ and $Ba_4ZnTi_{11}O_{27}$.

peaks. In contrast, in the present study the X-ray powder diffraction pattern of $BaFe_{12}O_{19}$ was essentially unchanged at all concentrations of TiO_2; significant shifts in lattice parameters were not observed. A large quadrilateral two-phase region between a corundum-type solid solution of TiO_2 in Fe_2O_3 and the $BaFe_{12}O_{19}$-type solid solution was observed, as shown in Fig. 2. A solubility limit of ≈13 mol% TiO_2 in Fe_2O_3 (i.e., $0.13TiO_2:0.87Fe_2O_3$) was indicated in the present study, in agreement with that reported by Webster and Bright (35) in air at 1200°C. $BaFe_{12}O_{19}$ was found to be in equilibrium with ten other compounds; hence, the properties of $BaFe_{12}O_{19}$ ceramics could be modified with those of these compounds by deliberate processing of compositions along the indicated two-phase joins.

Oxidation State of Iron

The presence of Fe^{4+} was clearly indicated near the high-BaO regions of the $BaO–Fe_2O_3–TiO_2$ system, as

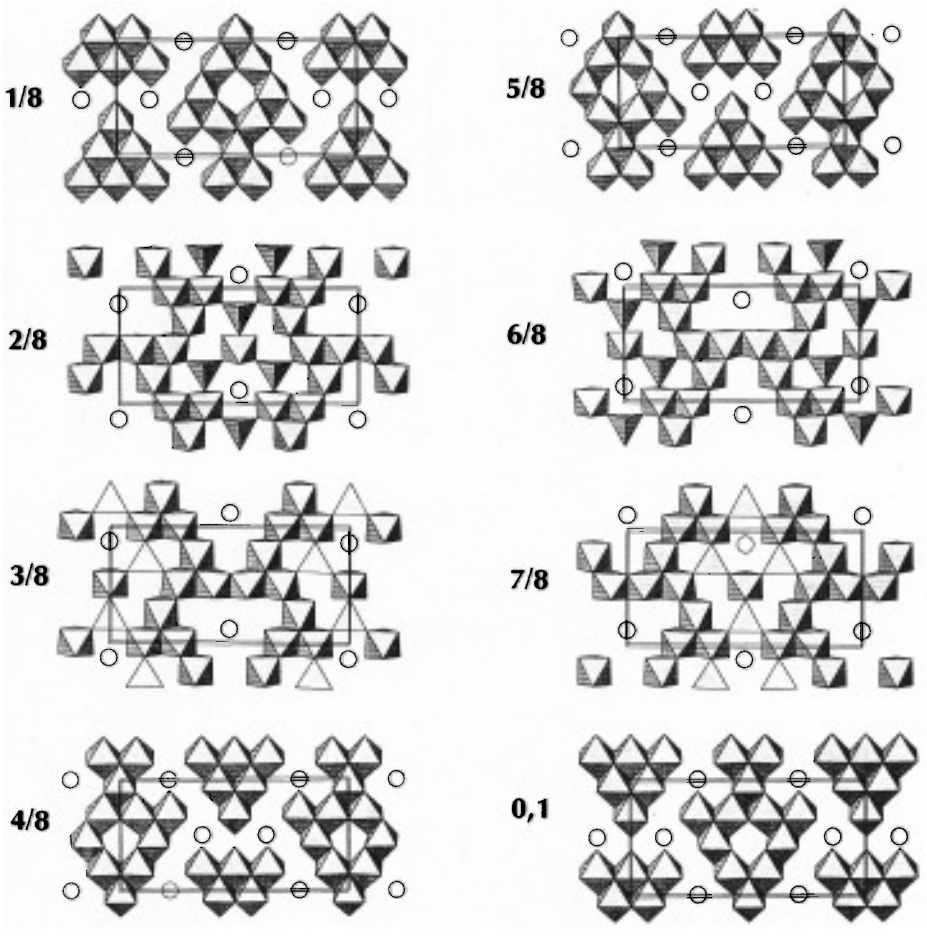

FIG. 7. The monoclinic crystal structure of $\approx Ba_3Fe_{24}Ti_7O_{53}$ (''3:12:7'') (Compound D, Table 1) viewed as layers along the distorted-close-packing *a* direction. Large spheres are Ba cations. The structure is a close-packed 8L arrangement with eighteen Fe^{3+}/Ti^{4+} sites, two of which feature tetrahedral coordination and appear to be preferentially occupied by Fe^{3+}.

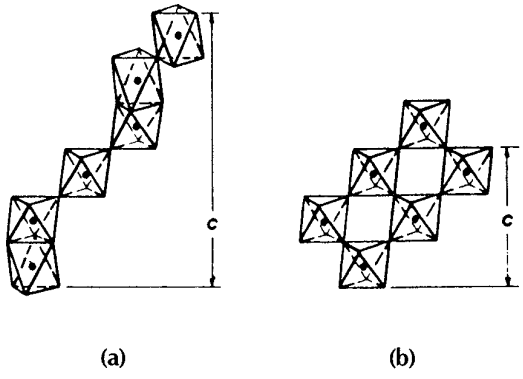

FIG. 8. Connectivity of octahedra in the (a) hexagonal $BaTiO_3$ and the (b) perovskite-like cubic/tetragonal $BaTiO_3$ structures (26). Face-sharing pairs of octahedra occur in the hexagonal form whereas in the cubic/tetragonal forms all octahedra share all vertices. The Ba cations have been omitted.

noted above for the hexagonal $BaTi_{1-x}Fe_xO_{3-z}$ solid solution. The remainder of the system is most likely characterized by Fe^{3+}, with no appreciable reduction to Fe^{2+}, for a number of reasons: The syntheses were carried out in air at 1250–1270°C, well below the $Fe_2O_3 \rightarrow Fe_3O_4$ conversion at 1400°C (61). Detailed structural characterization of $BaFe_4Ti_2O_{11}$, including powder neutron diffraction and Mössbauer spectroscopy (40), indicated that iron was present only in the trivalent state. Single-crystal structural studies of $Ba_{12}Fe_{28}Ti_{15}O_{84}$ (45) and the compounds described here have all indicated stoichiometric ratios and bond distances consistent with Fe^{3+}. Lastly, preliminary resistivity vs temperature measurements of sintered pellets of twelve high-iron compositions, including $BaFe_{12}O_{19}$, indicated nearly identical semiconducting curvatures (62). The oxidation-state behavior of iron in the $BaO–Fe_2O_3–TiO_2$ system appears to be the same as that reported for the $BaO–Fe_2O_3–SnO_2$ system (42).

Crystal Chemistry of the $BaO–Fe_2O_3–TiO_2$ System

The complex interior of the $BaO–Fe_2O_3–TiO_2$ phase diagram is attributable to the coincidence of three crystal-chemical factors: the size of Fe^{3+}, its electronic configuration, and the preference of Ba^{2+} to pack with oxygen ions to form close-packed layers. The ionic radius of Fe^{3+} and its radius ratio with O^{2-} (63, 21) facilitate its frequent occupation of four-, five-, and six-coordinated sites in oxide structures. Further, the high-spin d^5 electronic configuration of Fe^{3+} results in zero octahedral crystal field stabilization energy (21, 64). Finally, within close-packed O/Ba–O layers a large number of interstices exist. For every close-packed atom one octahedral site and two tetrahedral sites are formed; in addition, nearly an infinite number of stacking sequences of configured layers is possible. Further possibilities are generated upon distortion of the ideal packing to form five-coordinated sites. Hence, the versatile crystal-chemistry of Fe^{3+} along the boundaries of the ternary system ((4 + 2)-coordinated in Fe_2TiO_5; octahedral in corundum-type Fe_2O_3; four-, five-, and six-coordinated in $BaFe_{12}O_{19}$; strictly tetrahedral in $BaFe_2O_4$; and octahedral in $Ba_2Fe_2O_5$) is reflected in the interior of the $BaO–Fe_2O_3–TiO_2$ system. The large number of ternary compounds confirmed in the present study is therefore not unexpected. The formation of some of the ternary compounds, most notably 4:2:3, 3:2:3, and 6:2:7 $BaO–Fe_2O_3–TiO_2$, was found to be sluggish and influenced by kinetic factors such as identity of secondary phases and exact temperature. We conclude that other ternary compounds may exist in different temperature regions; i.e., the subsolidus $BaO–Fe_2O_3–TiO_2$ phase relations are unusually temperature dependent. This observation is also consistent with the versatile crystal-chemistry of Fe^{3+} and the opportunity to form a large number of close-packed layered structures with marginally different free energies of formation. At temperatures above those of the present study, the regions of the ternary diagram near BaO and Fe_2O_3 are likely to be strongly dependent on a fourth component, oxygen, as the oxidation state of Fe varies above and below 3+, respectively.

CONCLUSIONS

An investigation of the $BaO–Fe_2O_3–TiO_2$ ternary phase diagram by solid-state reaction at 1250–1270°C has confirmed the existence of fourteen previously unreported ternary compounds in addition to two of three ternary phases reported in the literature. Four of the new compounds were found to be isostructural with chemically similar known phases. The remaining ten adopt presumably new structure-types, one of which is described here. Using flux and neat melting methods, crystals of twelve of the fourteen new ternaries have been grown. Most of the compounds found in the interior of the $BaO–Fe_2O_3–TiO_2$ system were observed to be attracted to a small hand magnet; characterization of their magnetic and dielectric properties will be reported elsewhere. An extensive solid solution with the hexagonal $BaTiO_3$ structure was found for

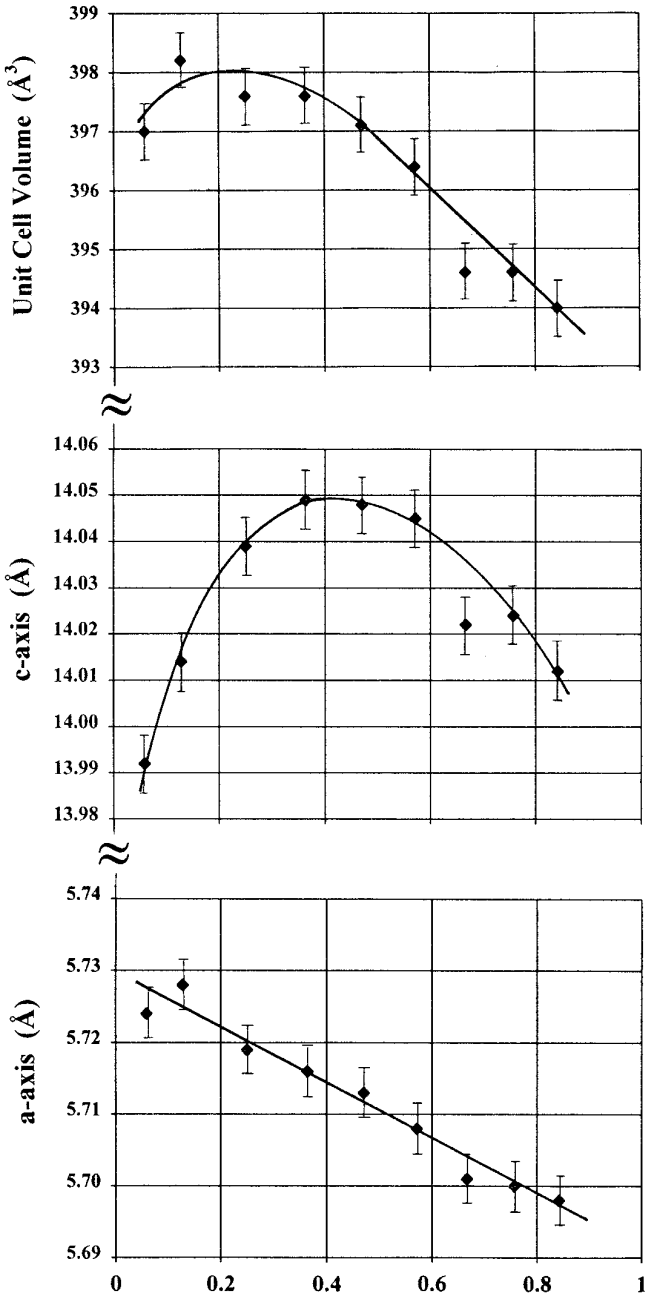

FIG. 9. Unit cell parameters and volume for the hexagonal $BaTiO_3$-type solid solution $BaTi_{1-x}Fe_xO_{3-z}$, $x = 0.06 \rightarrow 0.84$. Substitution of iron for Ti^{4+} can occur by oxidation to Fe^{4+} and/or by the formation of anion vacancies. The behavior of the lattice parameters shown here suggests that more than one process contributes to the formation of the solid solution, that these processes affect the lattice differently, and that the dominant process changes near an x value of 0.4. The curves shown here serve only as a guide for the eye.

$BaTi_{1-x}Fe_xO_{3-z}$, $x = 0.06 \rightarrow 0.84$, and was found by qualitative chemical analyses to contain tetravalent iron; this behavior is similar to that reported for the $BaO–Fe_2O_3–SnO_2$ system (42). The dependence of the hexagonal unit cell parameters on iron concentration was complex; both anion vacancy formation and oxidation to Fe^{4+} may contribute to formation of the $BaTi_{1-x}Fe_xO_{3-z}$ solid solution. Substantial solid solution regions were also found for the hollandite-type structure ($Ba_xFe_{2x}Ti_{8-2x}O_{16}$, $x = 1.07 \rightarrow 1.33$) and for TiO_2 dissolved in the $BaFe_{12}O_{19}$ structure (end member $BaFe_{10.8}Ti_{0.9}O_{19}$). In the present study no indications of divalent iron were observed.

ACKNOWLEDGMENTS

The authors are grateful to James P. Cline for his continuing technical support of the X-ray diffraction facilities. We appreciate the benefit of helpful discussions with Vicky L. Karen and Alan D. Mighell.

REFERENCES

1. G. Geiger, *Am. Ceram. Soc. Bull.* **73**(8), 57 (1994).
2. T. Abraham, *Am. Ceram. Soc. Bull.* **73**(8), 62 (1994).
3. T. Negas, R. S. Roth, H. S. Parker, and D. Minor, *J. Solid State Chem.* **9,** 297 (1974).
4. R. S. Roth, C. J. Rawn, C. G. Lindsay, and W. Wong-Ng, *J. Solid State Chem.* **104,** 99 (1993), and references cited therein.
5. D. E. Rase and R. Roy, *J. Am. Cearam. Soc.* **38,** 102 (1955).
6. H. M. O'Bryan, Jr., J. Thomson, Jr., and J. K. Plourde, *J. Am. Ceram. Soc.* **57,** 450 (1974).
7. H. M. O'Bryan, Jr. and J. Thomson, Jr., *J. Am. Ceram. Soc.* **57,** 522 (1974).
8. J. J. Ritter, R. S. Roth, and J. E. Blendell, *J. Am. Ceram. Soc.* **62,** 155 (1986).
9. R. S. Roth, J. J. Ritter, H. S. Parker, and D. B. Minor, *J. Am. Ceram. Soc.* **69,** 858 (1986).
10. K. W. Kirby and B. A. Wechsler, *J. Am. Ceram. Soc.* **74,** 1841 (1991).
11. F. W. Harrison, *Acta Crystallogr.* **9,** 495 (1956).
12. E. Tillmanns, *Acta Crystallogr. Sect. B* **25,** 1444 (1969).
13. E. Tillmanns, W. Hofmeister, and W. H. Baur, *J. Am. Ceram. Soc.* **66,** 268 (1983).
14. D. H. Templeton and C. H. Dauben, *J. Chem. Phys.* **32,** 1515 (1960).
15. E. Tillmanns, *Inorg. Nucl. Chem. Lett.* **7,** 1169 (1971).
16. E. Tillmanns and W. H. Baur, *Acta Crystallogr. Sect. B* **26,** 1645 (1970).
17. H. Arend and L. Kihlborg, *J. Am. Ceram. Soc.* **52,** 63 (1969).
18. J. Akimoto, Y. Gotoh, and Y. Osawa, *Acta Crystallogr. Sect. C* **50,** 160 (1994).
19. H. D. Megaw, *Proc. Phys. Soc. London* **58,** 133 (1946).
20. J. A. Bland, *Acta Crystallogr.* **14,** 875 (1961).
21. A. F. Wells, "Structural Inorganic Chemistry," 4th ed. Clarendon, Oxford, 1975.
22. Y. Goto and T. Takada, *J. Am. Ceram. Soc.* **43,** 150 (1960).
23. E. M. Levin, C. R. Robbins, and H. F. McMurdie (Eds.), "Phase Diagrams for Ceramists," Vol. I. American Ceramic Society, Columbus, 1964.
24. H. J. Van Hook, *J. Am. Ceram. Soc.* **47,** 579 (1964).
25. J. Li, T. M. Gür, R. Sinclair, S. S. Rosenblum, and H. Hayashi, *J. Mater. Res.* **9,** 1499 (1994).
26. O. Muller and R. Roy, "The Major Ternary Structural Families." Springer-Verlag, New York, 1974.
27. H. Mitsuda, S. Mori, and C. Okazaki, *Acta Crystallogr. Sect. B* **27,** 1263 (1971).
28. X. D. Zou, S. Hovmöller, M. Parras, J. M. González-Calbet, M. Vallet-Regí, and J. C. Grenier, *Acta Crystallogr. Sect. A* **49,** 27 (1993), and references cited therein.
29. M. Parras, M. Vallet-Regí, J. M. González-Calbet, M. A. Alario-Franco, J. C. Grenier, and P. Hagenmuller, *Mater. Res. Bull.* **22,** 1413 (1987).
30. G. Sloccari, *J. Am. Ceram. Soc.* **56,** 489 (1973).
31. R. S. Roth, T. Negas, and L. P. Cook (Eds.), "Phase Diagrams for Ceramists," Vol. IV. American Ceramic Society, Columbus, 1981.
32. A. E. McHale (Ed.), "Phase Diagrams for Ceramists," Annual '91. American Ceramic Society, Columbus, 1964.
33. S. Mori, *J. Am. Ceram. Soc.* **49,** 600 (1966).
34. T. Negas and R. S. Roth, *J. Res. Natl. Bur. Stand. Sect. A* **73,** 425 (1969).
35. A. H. Webster and N. F. H. Bright, *J. Am. Ceram. Soc.* **44,** 110 (1961).
36. M. D. Karkhanavala and A. C. Momin, *J. Am. Ceram. Soc.* **42,** 399 (1959).
37. I. E. Grey and L. A. Bursill, *Acta Crystallogr. Sect. B* **34,** 2412 (1978).
38. W. H. Baur, *Mater. Res. Bull.* **16,** 339 (1981).
39. F. Haberey and M. Velicescu, *Acta Crystallogr. Sect. B* **30,** 1507 (1974).
40. X. Obradors, A. Collomb, J. Pannetier, A. Isalgué, J. Tejada, and J. C. Joubert, *Mater. Res. Bull.* **18,** 1543 (1983).
41. Software by Eric Dowty, ATOMS for Windows; Shape Software, 521 Hidden Valley Road, Kingsport, TN 37663; 74457.1703@compuserve.com.
42. M. C. Cadée and D. J. W. Ijdo, *J. Solid State Chem.* **36,** 314 (1981).
43. N. P. Belikaya, E. I. Grindin, M. A. Kvantov, Yu. P. Kostikov, and G. D. Rubal'skii, *Inorg. Mater.* (*Engl. Transl.*) **21,** 243 (1985).
44. Powder Diffraction File, International Centre for Diffraction Data, Newtown Square, Pennsylvania; patterns 20-129, 39-810, 39-1296.
45. I. E. Grey, A. Collomb, and X. Obradors, *J. Solid State Chem.* **91,** 131 (1991).
46. H. W. Zandbergen and D. J. W. Ijdo, *Mater. Res. Bull.* **18,** 371 (1983).
47. M. C. Cadée and G. C. Verschoor, *Acta Crystallogr. Sect. B* **34,** 3554 (1978).
48. C. G. Lindsay, C. J. Rawn, and R. S. Roth, *Powder Diffr.* **9,** 56 (1994).
49. Program CELLSVD by C. K. Lowe-Ma, Naval Air Warfare Center Weapons Division Technical Publication 8128, September 1993.
50. Software by W. Craig Carter, wcraig@pruffle.nist.gov; to be available as public domain software: http::/www.ctcms.nist.gov.
51. J. P. Cline, A. R. Drews, and T. A. Vanderah, submitted for publication.
52. B. G. Hyde and S. Andersson, "Inorganic Crystal Structures." Wiley, New York, 1989.
53. T. A. Vanderah, Q. Huang, W. Wong-Ng, B. C. Chakoumakos, R. B. Goldfarb, R. G. Geyer, J. Baker-Jarvis, R. S. Roth, and A. Santoro, *J. Solid State Chem.* in press.
54. J. P. Cline and T. A. Vanderah, submitted for publication.
55. T. A. Vanderah, W. Wong-Ng, R. S. Roth, R. G. Geyer, and R. B. Goldfarb, submitted for publication.
56. H. Vinek, H. Völlenkle, and H. Nowotny, *Monatsh. Chem.* **101,** 275 (1970).

57. J. Schmachtel and Hk. Müller-Buschbaum, *Z. Anorg. Allg. Chem.* **472,** 89 (1981).
58. C. S. Barrett, ''Structure of Metals.'' McGraw-Hill, New York, 1943.
59. H. D. Megaw, *Nature* **155,** 484 (1945).
60. G. Heimke, *J. Appl. Phys.* **31,** 271S (1960).
61. N. N. Greenwood and A. Earnshaw, ''Chemistry of the Elements.'' Pergamon, New York, 1984.
62. M. S. Osofsky, Naval Research Laboratory, private communication.
63. R. D. Shannon, *Acta Crystallogr. Sect. A* **32,** 751 (1976).
64. F. A. Cotton and G. Wilkinson, ''Advanced Inorganic Chemistry,'' 4th ed. Wiley, New York, 1980.